High-Efficiency Nanosecond Green Laser Based on Extra-Cavity Second-Harmonic Generation of a Nd:YAG MOPA System

Hua-Yu Liu, Zi-Han Zhou, Qi Bian, Yong Bo, Yang Kou, Lei Yuan, Da-Fu Cui, and Qin-Jun Peng

***Abstract*—A high infrared-to-green conversion efficiency laser is demonstrated by extra-cavity frequency-doubling of a master oscillator power amplifier (MOPA) laser. The oscillator is a diode-side-pumped acousto-optic Q-switched Nd:YAG laser at 1064 nm with an average output power of 38.2 W and a beam quality factor $M^2 = 1.15$, operating at a 2 kHz repetition rate and a 38.3 ns pulse duration. After a dual-rod double-pass amplifier, the fundamental seed power is amplified to 89.4 W with the beam quality of $M^2 = 1.41$ and pulse duration of 56.4 ns. Using a type I lithium triborate (LiB_3O_5, LBO) crystal for second-harmonic generation (SHG), an average power of 67.4 W at 532 nm is generated with a beam quality factor of 1.31, operating at 41.8 ns of pulse duration. The corresponding frequency doubling efficiency is as high as 75.4%, which is, to the best of our knowledge, the highest doubling efficiency reported ever for 532 nm source by an extra-cavity SHG laser system.**

***Index Terms*—Green laser, high-efficiency, Nd:YAG MOPA, extra-cavity frequency doubling.**

I. Introduction

HIGH average power solid-state green lasers are attractive for various demands in scientific and industrial applications, such as laser deep engraving [1], precision micro-machining [2], laser annealing [3], biomedical research [4], [5], molecular photo-switch [6], solar cell manufacturing [7], optical parameter oscillators [8], pumping sources for Ti:sapphire laser [9] and ocean exploration [10]. In general, the second-harmonic generation (SHG) from a fundamental beam (FB) near infrared radiation (NIR) around 1 μm wavelength is always used to achieve green source. Compared with intra-cavity frequency doubling [11], extra-cavity frequency doubling of master oscillator power amplifier (MOPA) system is most widely used to produce high power SHG output with high beam quality, for its low thermal perturbation and easy-to-implement structure [12].

Manuscript received 7 May 2023; revised 18 August 2023; accepted 24 August 2023. Date of publication 28 August 2023; date of current version 8 September 2023. This work was supported by the National Outstanding Youth Science Fund Project of National Natural Science Foundation of China under Grant 62005295. *(Corresponding authors: Qi Bian; Yong Bo.)*

Hua-Yu Liu and Zi-Han Zhou are with the Key Lab of Solid State Laser, Technical Institute of Physics and Chemistry, Chinese Academy of Sciences, Beijing 100190, China, and also with the University of Chinese Academy of Sciences, Beijing 100190, China.

Qi Bian, Yong Bo, Yang Kou, Lei Yuan, Da-Fu Cui, and Qin-Jun Peng are with the Key Lab of Solid State Laser, Technical Institute of Physics and Chemistry, Chinese Academy of Sciences, Beijing 100190, China, and also with the Institute of Optical Physics and Engineering Technology, Jinan 250000, China (e-mail: bianqi@mail.ipc.ac.cn; boyong@tsinghua.org.cn).

Digital Object Identifier 10.1109/JPHOT.2023.3309390

With the extra-cavity SHG, for example, a nanosecond (ns) 1064 nm-to-532 nm conversion efficiency of 44.7% with 30 W average power output and a beam quality factor of $M^2 = 1.6$ was demonstrated at a pulsed duration of 5 ns and a pulse repetition rate (PRR) of 100 kHz [13]. Recently, a few sub-ns pulse 532 nm lasers have also been reported [14], [15]. For instance, a SHG conversion efficiency of 61.8% was realized from a laser diode (LD) end-pumped Nd:YVO_4 MOPA system running at 1 kHz, delivering an average power of 40.5 W with a beam quality factor of $M^2 = 1.26$ [15]. In another work, 63.5% SHG efficiency from a LD side-pumped electro-optic Q-switched Nd:YAG MOPA laser was obtained with the SH average power of 50.2 W at 532 nm. However, the divergence angle was about 0.6 mrad, corresponding to a beam quality factor of $M^2 \sim 9.7$ [16]. Up to 67% SHG efficiency with 103.5 W at 532 nm was obtained by a FB 4-stage Nd:YVO_4 amplifier at 60 kHz PRR and 11.8 ns pulse width, the 532 nm beam quality factor was $M^2 = 1.34$ [17]. Accordingly, this was the highest frequency doubling efficiency for SHG 532 nm radiation so far. On the other hand, for the 515 nm green light from frequency-doubled 1030 nm Yb:YAG laser, higher SHG efficiency was implemented [18], [19]. Very recently, a conversion efficiency of 71% was achieved based on two cascaded Yb:YAG thin-disk multi-pass amplifiers at a wavelength of 1030 nm [18]. Soon after, another higher conversion efficiency of 89% from 1030 nm-to-515 nm was achieved from a cryogenically cooled Yb:YAG slabs amplifier system and frequency doubling in two LiB_3O_5 (LBO) crystals [19]. Unfortunately, both of the two FB MOPA laser systems were rather complex, bulky and costly, which limits their applicability. The above-mentioned reports provide incredibly useful information, but it still remains a challenge to enhance the NIR-to-green efficiency together with good beam quality and relatively simple structure.

In this paper, based on a compact extra-cavity SHG of Nd:YAG MOPA FB laser in LBO crystal, a high SH conversion efficiency from 1064 nm to 532 nm is achieved by optimizing the size of the FB and the length of nonlinear crystal. At a maximum FB power of 89.4 W, a SH power of 67.4 W is created, which corresponds to a conversion efficiency of up to 75.4%. To the best of our knowledge, this is the first report to date on the SHG 532 nm source with the conversion efficiency of more than 70%. The 532 nm laser operates at a PRR of 2 kHz and pulse duration of 41.8 ns, resulting in a pulse energy of $\sim$ 34 mJ. A good SH beam quality is measured to be $M^2 = 1.31$.

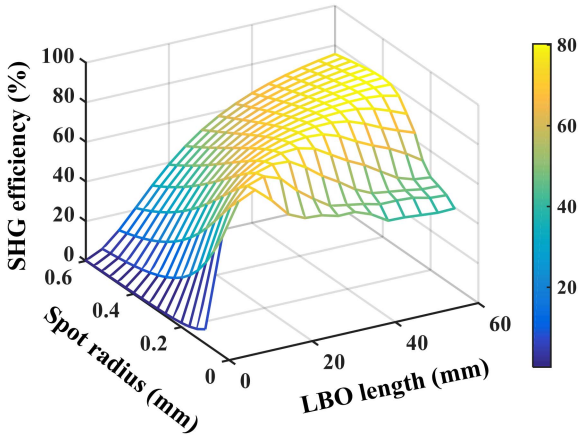

Fig. 1. SHG efficiency versus the LBO crystal length and FB radius under pump power of 89.4 W.

II. Numerical SHG Model

In order to obtain high SHG conversion efficiency from the 1064 nm-to-532 nm, the FB size as well as the nonlinear crystal length should be optimized. A modified non-critical phase matching (NCPM) SHG theoretical model based on coupled-wave equations describing propagation for ns pulses is introduced below [20]. The SHG equations have taken the pump depletion and linear absorption into account and without considering the beam spatial birefringent walk-off as the adoption of NCPM:

$$\frac{\partial E_1(x,y,z,t)}{\partial z} = j\sigma_1 E_2 E_1^* \exp(j\Delta kz) - \frac{\gamma_1}{2} E_1(x,y,z,t) \tag{1}$$

$$\frac{\partial E_2(x,y,z,t)}{\partial z} = j\sigma_2 E_1^2 \exp(-j\Delta kz) - \frac{\gamma_2}{2} E_2(x,y,z,t) \tag{2}$$

where E_1 and E_2 are spatial and temporal complex amplitudes of the FB and SH beam, respectively. Δk is the wave vector mismatch value, and its value is 0 due to NCPM setup. $\sigma_{1,2} = \omega d_{eff}/cn_{1,2}$ is the coupling coefficient of the second-order nonlinear pulse. ω is the angle frequency of the FB wavelength, $d_{eff} = 0.85$ pm/V is the effective nonlinear coefficient of LBO crystal, $n_{1,2} = 1.605$ for the NCPM is the refractive indices of LBO crystal at the FB and SH wavelength, c is the speed of light in vacuum, γ_1 and γ_2 are linear absorption coefficient at the 1064 nm and 532 nm in the LBO, respectively. By the Fourier transform and 4-order Runge-Kutta method, the above equations can be solved numerically. Assuming the Gaussian beam spatial and temporal profiles for the FB optical pulse, the evolution of the SH conversion efficiency with the length of LBO crystal and the radius of the fundamental spot under available maximum FB pump power of 89.4 W (see below) is simulated and the corresponding three-dimensional (3D) plot is shown in Fig. 1. It provides a basis for the optimization of the length of frequency doubling crystal and the FB size in the experiment. Some typical curves are taken from Fig. 1, and are shown in Fig. 2, i.e., the SHG efficiency as a function of LBO crystal length with different FB radii of 0.3, 0.4, 0.5 and 0.6 mm, respectively. By considering

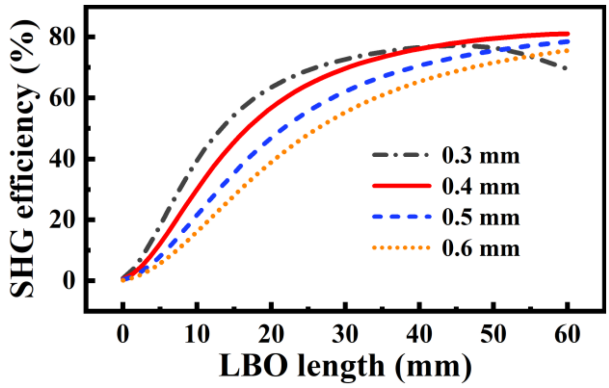

Fig. 2. SHG efficiency as a function of LBO crystal length for different FB radii under FB pump power of 89.4 W.

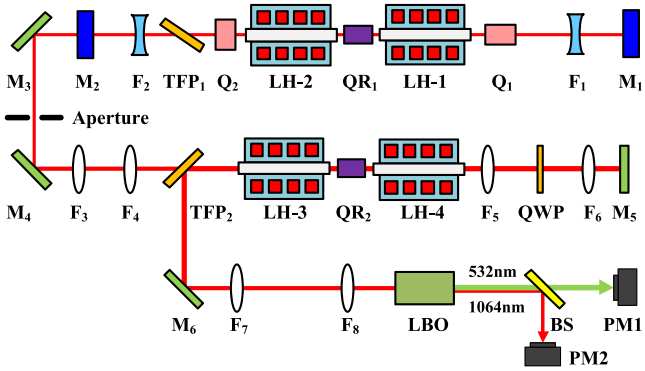

Fig. 3. Schematic diagram of the experimental arrangement for SHG laser system. LH-1 and LH-2, laser modules; QR_1 and QR_2, quartz rotators; F_1 and F_2, concave lenses; TFP_1 and TFP_2, thin-film polarizers; Q_1 and Q_2, Q-switch modulators; M_1 and M_3–M_6, high reflective (HR) mirrors; M_2, output coupler; F_3–F_8, beam shaping lenses; LH-3 and LH-4, amplification modules; QWP, quarter-wave plate; LBO, frequency doubling crystal; BS, beam splitter; PM1 and PM2, power meters.

a trade-off between a high SHG efficiency and the risk of optical damage in the LBO crystal for long term stable operation, we choose a radius of 0.4 mm for the FB and 40 mm long for the LBO crystal in the following experiment. Then, a high SHG efficiency of $> 75\%$ can be expected as seen in Fig. 2.

III. Experimental Setup

The overall experimental setup of the all-solid-state green laser system is schematically illustrated in Fig. 3, including an acousto-optic (AO) Q-switched Nd:YAG oscillator, a dual-rod double-pass Nd:YAG amplifier, and a LBO frequency doubler. In oscillator stage, a plane-plane linear cavity structure acts as the ns seed source. LH-1 and LH-2 are two identical Nd:YAG rod laser modules. Each Nd:YAG rod (Φ 3 mm $\times$ 82 mm) is doped with Nd^{3+} at a concentration of 0.6 at.%, whose end facets are anti-reflective (AR) coated at 1064 nm. Each rod is side-pumped in three-fold symmetric directions by quasi-continuous-wave (QCW) pulsed LD arrays at 808 nm. Compared with CW pumping, the operation of QCW pulsed diode-pump is used for reducing the thermal effects of the Nd:YAG crystal rods, which contributes to generate more energetic pulse with good beam quality. The pump PRR and pulse width are 2 kHz and 100 μs,

respectively. A quartz rotator QR_1 is placed between the LH-1 and LH-2 to compensate the thermally induced birefringence in the dual-rods for improving the overall beam quality. Two concave lenses F_1 and F_2 with equal focal lengths of -75 mm are placed in the cavity to enlarge the volume of the fundamental mode and filter out the higher-order transverse modes, for obtaining a good TEM_{00} mode. A polarizer TFP_1 is coated with high transmission (HT) film for parallel direction and HR film for vertical direction at Brewster's angle of 55.6°. While a horizontal polarized light is incident on the TFP_1 at Brewster's angle, there is no reflection loss for efficiently providing the linearly polarized seed beam. Two AO modulators Q_1 and Q_2 are operating at compressional acoustic waves, which have higher diffraction loss at a linearly polarized laser with vertical to base. Due to the 90° rotation of the laser polarization state by QR_1, AO Q-switches with a total radio frequency power of 100 W are inserted orthogonally to each other in the front of LH-1 and behind of LH-2 to increase the diffraction loss in the vertical and parallel directions, thus enhancing the switch-off capability for generating high peak power ns pulses. The rear mirror M_1 is coated with HR film at 1064 nm, and the output coupler mirror M_2 is coated with partial transmission film of 70% at 1064 nm.

To further scale the fundamental power, a dual-rod double-pass amplifier architecture equipped with two laser amplification modules and a quartz rotator, both same as to the oscillator stage is constructed. Plane mirror M_3 and M_4 are HR coated at 1064 nm with an incident angle of 45°. An aperture is adopted to ensure good beam quality through filtering out the stray light of Gaussian beam. Lenses F_3 to F_6 are used to match the beam size to the Nd:YAG rods in LH-3 and LH-4 to maximize the extraction efficiency. A quarter-wave plate QWP is used to adjust the polarization state of the laser beam to orthogonal direction after passing through the amplifier twice. TFP_2 is HT coated for parallel direction and HR coated for vertical direction with an incidence angle of 45° at 1064 nm, for injection of the seed beam and switching out of the amplified FB. Plane mirror M_5 is coated with HR film at 1064 nm at an incident angle of 0°. Eventually, a second pass amplification is achieved with the combination of QWP, TFP_2 and M_5.

In the SHG stage, the amplified FB is reflected by mirror M_6, and then injected into the LBO crystal to achieve single-pass SHG with a wavelength of 532 nm. Two lenses F_7 and F_8 are used to adjust the spot size of the collimated beam inside the LBO crystal to obtain high nonlinear conversion efficiency without damaging the coatings. As the frequency doubling crystal, LBO is considered as a suitable choice for its good mechanical characteristics, large acceptance angle and high damage threshold [17]. The type-I NCPM LBO crystal with $4 \times 4 \times 40$ mm^3 in size is cut at $\theta = 90°$, $\phi = 0°$, which is longer than that of Ref. [15] (20 mm length) and Ref. [16] (25 mm length). The both end surfaces of the LBO are AR coated at 1064 and 532 nm, and is held in a resistively heated oven with the actively controlled temperature set at 145.6 $\pm$ 0.05 °C to achieve the type-I NCPM with wide acceptance angle, no spatial walk-off, and high effective nonlinear optics coefficient. Beam splitter BS is coated with the HT film at 532 nm and HR film at 1064 nm to separate the residual FB from the green beam. Two power meters PM1 and PM2 are employed to measure the output power of green and NIR laser, respectively.

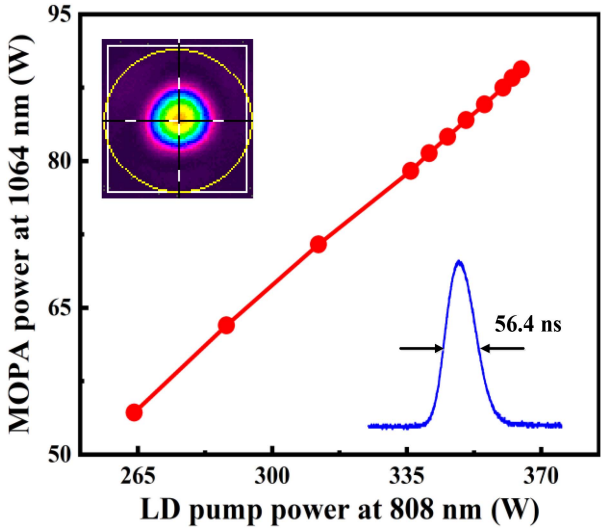

Fig. 4. Output power of MOPA system laser at 1064 nm versus total pump power of amplifier. Lower right inset: Pulse width of the amplified laser; upper left inset: 2-D beam spatial profile of the amplified beam.

In the experiment, the PM1 and PM2 are two identical power meters (OPHIR FL300A). The pulse temporal waveform characteristics is monitored by a high-speed photodetector (ALPHALAS GMBH, UVIR-P, rise time $<$ 40 ps) connected to a 1 GHz bandwidth digital oscilloscope (Agilent, DPO 4014B-L). A beam quality analyzer M^2-200 (Spiricon Inc.) is measured the beam quality factor M^2 as well as the two-dimensional (2D) and 3D beam spatial profiles. And, the laser spectrum is tested based on an optical spectrum analyzer (AvaSpec-2048FT-SPU).

IV. Results and Discussion

The compact oscillator system has achieved a maximum average output power of 38.2 W under the LD pump power of 367.2 W at 808 nm, operating at a PRR of 2 kHz with a pulse width of 38.3 ns is attained. The seed light simultaneously features a good beam quality factor of $M^2 = 1.15$, indicating a good Gaussian spatial mode operation. To further generate a high power 1064 nm laser for SHG, a 38.2 W seed beam is injected into LD side-pumped Nd:YAG double-pass amplifier system. The amplified FB output power is depicted in Fig. 4, which grows linearly and increased up to 89.4 W under the pump power of 364.8 W. In the lower right inset of Fig. 4, a pulse temporal width of the amplifying NIR radiation is captured to expand to 56.4 ns. In the upper left inset of Fig. 4, a distributed 2D beam spatial intensity profile is measured under the maximum NIR output, suggesting that the amplifier system maintains good beam quality with smooth beam pattern, which facilitates the enhancement of SHG efficiency. And, the average M^2 value of amplified FB is measured to be 1.41 at full output power.

In the SHG stage, through optimizing the focal lengths of F_7 and F_8 lenses, the 1064 nm FB is collimated to be $\sim$ 800 μm diameter instead of a focused beam in the LBO crystal. Fig. 5 shows the SH output power and conversion efficiency of the

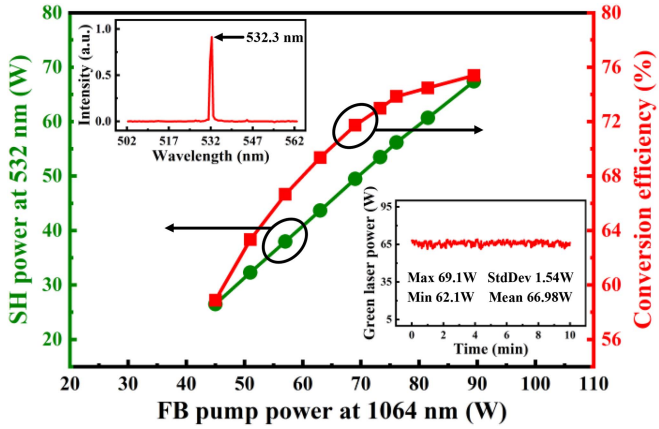

Fig. 5. SH power at 532 nm and conversion efficiency versus FB pump power at 1064 nm. Upper left inset: Measured SH spectrum. Lower right inset: Power stability test over 10 min at full output power.

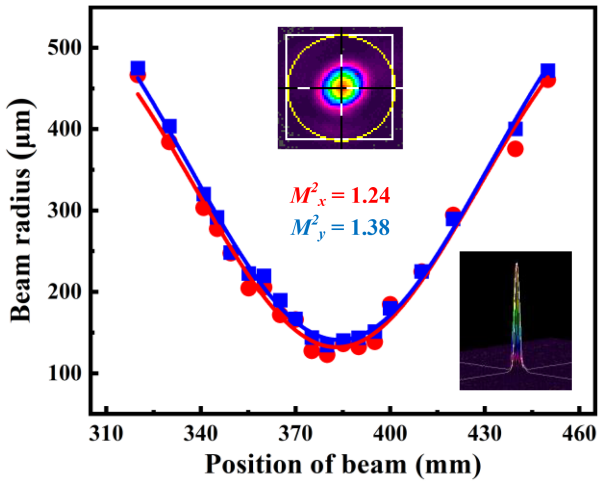

Fig. 6. Measured beam quality factors of the 532 nm laser at maximum output power. Upper middle inset: 2-D beam spatial profile. Lower right inset: 3D beam spatial profile.

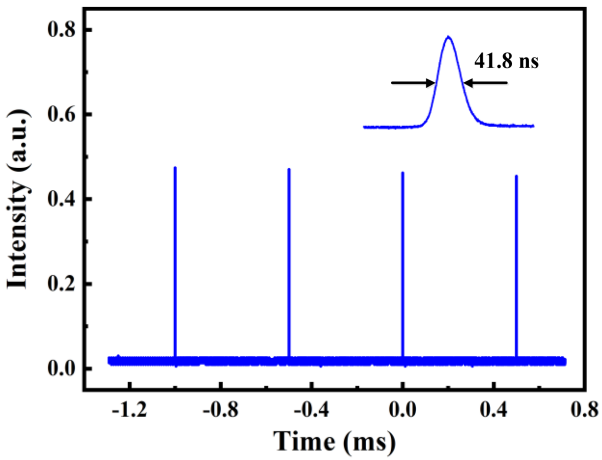

Fig. 7. Typical pulse waveforms of the Q-switched 532 nm laser. Inset: Temporally expanded profile of a single pulse.

green laser as a function of NIR input power. It can be seen that they remain monotonically rising with increasing FB pump power and without saturation behavior is observed, indicating a trend that higher doubling power and SHG efficiency could be attained by further increment of FB pump power. A highest SH output power of 67.4 W is obtained at an input FB power of 89.4 W, which corresponds to a SHG conversion efficiency up to 75.4%. With further increasing the LD pumping power, it is observed that the film on the end face of the LBO crystal is damaged due to the high input power intensity. To the best of our knowledge, this result presents the highest efficiency with more than 70% that has ever been reported through an extra-cavity SHG from 1064 nm-to-532 nm solid lasers.

The SH spectrum at full output power is exhibited in upper left inset Fig. 5, which depicts that the center wavelength is located at 532.3 nm. Furthermore, the stability of the green power is measured around the maximum output power, as shown in the lower right inset of Fig. 5. It is found that the power fluctuation is $\pm$ 2.3% (Std. Dev.) over 10 min. This indicates that the green laser system operates in a stable and reliable setup, which is a prerequisite for practical applications.

The beam quality of 532 nm laser is measured and shown in Fig. 6. The fitting of the experimental beam position points reveals the laser beam quality factors to be $M_x^2 = 1.24$ in the x axis and $M_y^2 = 1.38$ in the y axis, corresponding to an average M^2 value of 1.31. The upper middle inset and lower right inset in Fig. 6 display the 2D and 3D intensity profile of the SH beam, respectively. Obviously, the 532 nm laser is operating in good Gaussian mode with round spot cross section and smooth intensity-distribution curve. Compared to the input FB, the M^2 value of the SH beam is slightly better resulting from the intensity-dependent conversion efficiency during the SHG process.

The temporal waveform characteristics of the 532 nm pulse laser at the maximum output power are recorded in Fig. 7, which depicts the typical laser pulse train with a PRR of 2 kHz. The pulse-pulse amplitude fluctuation is calculated to be within $\pm$ 1.9%. The inset in Fig. 7 displays an expanded profile of a single SH pulse with the pulse width of 41.8 ns, which is narrower around a factor of $\sqrt{2}$ than that of the input pump FB pulse as expected due to the temporal gain narrowing effect [21]. Consequently, the 532 nm laser provides a high pulse energy of up to $\sim$ 34 mJ and a high peak power of up to 0.8 MW.

V. Conclusion

A high SHG efficiency, high pulse energy, ns 532 nm laser with good beam quality is demonstrated. The green 532 nm radiation is achieved based on an extra-cavity frequency-doubling of a Q-switched 1064 nm Nd:YAG MOPA laser in the LBO crystal. At FB power of 89.4 W, a maximum average power of 67.4 W at 532 nm is obtained with good beam quality of $M^2 = 1.31$, operating at a PRR of 2 kHz and pulse width of 41.8 ns, which implies a high pulse energy of $\sim$ 34 mJ. The 1064 nm-to-532 nm conversion efficiency is calculated to be 75.4%. We believe that this is the highest efficiency 532 nm green laser for extra-cavity SHG solid lasers.

REFERENCES

[1] C. Leone, V. Lopresto, and I. D. Iorio, "Wood engraving by Q-switched diode-pumped frequency-doubled Nd: YAG green laser," *Opt. Lasers Eng.*, vol. 47, no. 1, pp. 161–168, 2009, doi: 10.1016/j.optlaseng.2008.06.019.

[2] P. Jaworski et al., "High energy green nanosecond and picosecond pulse delivery through a negative curvature fiber for precision micro-machining," *Opt. Exp.*, vol. 23, no. 7, pp. 8498–8506, 2015, doi: 10.1364/OE.23.008498.

[3] S. M. Jung et al., "Selective annealing of Al_2O_3/silicon interface by using an Nd^{3+}:YAG laser with a wavelength of 532 nm," *Mater. Sci. Semicond. Process.*, vol. 109, 2020, Art. no. 104956, doi: 10.1016/j.mssp.2020.104956.

[4] G. Klinda et al., "532 nm laser treatment of molluscum contagiosum," *Med. Laser Appl.*, vol. 26, no. 4, pp. 172–175, 2011, doi: 10.1016/j.mla.2011.08.005.

[5] M. S. Choi et al., "Effects of picosecond laser on the multi-colored tattoo removal using Hartley Guinea pig: A preliminary study," *PLoS One*, vol. 13, no. 9, 2018, Art. no. e0203370, doi: 10.1371/journal.pone.0203370.

[6] J. Garcia-Amorós et al., "New heterocyclic systems to afford microsecond green-light isomerisable azo dyes and their use as fast molecular photochromic switches," *Chem. Commun.*, vol. 49, no. 97, pp. 11427–11429, 2013, doi: 10.1039/c3cc46736h.

[7] D. R. Dudley et al., "Q-switched diode-pumped Nd:YAG rod laser with output power of 420W at 532nm and 160W at 355nm," *Proc. SPIE*, vol. 7193, pp. 261–268, 2009, doi: 10.1117/12.808345.

[8] F. Kienle et al., "Green-pumped, picosecond MgO:PPLN optical parametric oscillator," *J. Opt. Soc. Amer. B*, vol. 29, no. 1, pp. 144–152, 2011, doi: 10.1364/JOSAB.29.000144.

[9] X. Ding et al., "Generation of 3.5W high efficiency blue-violet laser by intracavity frequency-doubling of an all-solid-state tunable Ti:Sapphire laser," *Opt. Exp.*, vol. 16, no. 7, pp. 4582–4587, 2008, doi: 10.1364/OE.16.004582.

[10] D. Xu et al., "104 W high stability green laser generation by using diode laser pumped intracavity frequency-doubling Q-switched composite ceramic Nd:YAG laser," *Opt. Exp.*, vol. 15, no. 7, 2007, Art. no. 3991, doi: 10.1364/OE.15.003991.

[11] S. B. Zhang et al., "High electrical-to-green efficiency high stability intracavity-frequency-doubled Nd:YAG-LBO QCW 532 nm laser with a straight cavity," *Laser Phys. Lett.*, vol. 7, no. 10, pp. 707–710, 2010, doi: 10.1002/lapl.201010050.

[12] A. V. Hicks et al., "Advances in high-power diode-pumped ultraviolet lasers," *Proc. SPIE*, vol. 5332, pp. 120–133, 2004, doi: 10.1117/12.537912.

[13] J. He et al., "30 W output of short pulse duration nanosecond green laser generated by a hybrid fiber-bulk MOPA system," *Laser Phys.*, vol. 21, no. 4, pp. 708–711, 2011, doi: 10.1134/S1054660X11070115.

[14] G. Li et al., "Lidar-radar for underwater target detection using a modulated sub-nanosecond Q-switched laser," *Opt. Laser Technol.*, vol. 142, 2021, Art. no. 107234, doi: 10.1016/j.optlastec.2021.107234.

[15] Y. Huang et al., "A high peak power and high beam quality sub-nanosecond Nd: YVO_4 laser system at 1 kHz repetition rate without SRS process," *Appl. Sci.*, vol. 9, no. 23, 2019, Art. no. 5247, doi: 10.3390/app9235247.

[16] Z. Bai et al., "50.2W high stability and high compact all-solid-state green laser with extra-cavity frequency-doubling at 500 Hz," *Opt. Rev.*, vol. 20, no. 4, pp. 303–307, 2013, doi: 10.1007/s10043-013-0055-9.

[17] Q. Liu et al., "103 W high beam quality green laser with an extra-cavity second harmonic generation," *Opt. Exp.*, vol. 16, no. 19, pp. 14335–14340, 2008, doi: 10.1364/OE.16.014335.

[18] C. Röcker et al., "Ultrafast green thin-disk laser exceeding 1.4 kW of average power," *Opt. Lett.*, vol. 45, no. 19, pp. 5522–5525, 2020, doi: 10.1364/OL.403781.

[19] H. Chi et al., "Demonstration of a kilowatt average power, 1 J, green laser," *Opt. Lett.*, vol. 45, no. 24, pp. 6803–6806, 2020, doi: 10.1364/OL.412975.

[20] F. Yang et al., "Theoretical and experimental investigations of nanosecond 177.3," *Appl. Phys. B*, vol. 96, pp. 415–422, 2009, doi: 10.1007/s00340-009-3506-z.

[21] P. K. Mukhopadhyay et al., "Analysis of laser-diode end-pumped intracavity frequency-doubled, passively Q-switched and mode-locked Nd: YVO_4 laser," *Appl. Phys. B*, vol. 79, pp. 713–720, 2004, doi: 10.1007/s00340-004-1626-z.